PCCP

Role of Sterics in Phosphine-Ligated Gold Clusters

Journal:	*Physical Chemistry Chemical Physics*
Manuscript ID	CP-ART-08-2018-004961
Article Type:	Paper
Date Submitted by the Author:	03-Aug-2018
Complete List of Authors:	Parrish, Katherine; Grinnell College, Department of Chemistry King, Mary; University of Texas at Austin, Department of Chemistry Ligare, Marshall; PNNL, Chemical Physics and Analysis Johnson, Grant; Pacific Northwest National Laboratory, Chemical Physics and Analysis Hernandez, Heriberto; Grinnell College, Department of Chemistry

Role of Sterics in Phosphine-Ligated Gold Clusters

*Katherine A. Parrish,[a] Mary King,[b] Marshall R. Ligare,[c] Grant E. Johnson,[c] and Heriberto Hernández[a]**

[a]Department of Chemistry, Grinnell College, 1116 Eight Ave., Grinnell, IA 50112.

[b]Department of Chemistry, University of Texas at Austin, NMS 3.316, 2506 Speedway STOP A5300 Austin, TX 78712.

[c]Physical Sciences Division, Pacific Northwest National Laboratory, P.O. Box 999, MSIN K8-88, Richland, WA 99352.

*E-mail: hernandh@grinnell.edu

ABSTRACT

This study examined the solution-phase exchange reactions of triphenylphosphine (PPh_3) ligands on $Au_8L_7^{2+}$ (L = PPh_3) gold clusters with three different tolyl ligands using electrospray ionization mass spectrometry to provide insight into how steric differences in the phosphines influence the extent of ligand exchange and the stability of the resulting mixed-phosphine clusters. The size distributions of tolyl-exchanged gold clusters were found to depend on the position of the methyl group in the tri(tolyl)phosphine ligands (-ortho, -meta, and -para). Due to different sterics, the tri(m-tolyl)phosphine (TMTP) and tri(p-tolyl)phosphine (TPTP) ligands exchanged efficiently onto the $Au_8L_7^{2+}$ (L = PPh_3) clusters while the tri(o-tolyl)phosphine ligands did not exchange. In addition, while TPTP fully exchanged with all seven PPh_3 on the $Au_8L_7^{2+}$ cluster, TMTP exchanged with only six PPh_3 ligands. Employing collision-induced dissociation, the tolyl-exchanged mixed-ligand clusters were demonstrated to fragment through loss of neutral ligands and AuL_2^+. Comparison of the relative fragmentation yields of PPh_3 *vs.* TMTP and TPTP from the mixed-ligand clusters indicated that these tolyl ligands are more strongly bonded to the Au_8^{2+} gold core than PPh_3. To provide molecular-level insight into the experimental results we also performed complementary electronic structure calculations using density functional theory at the B3LYP-D3/SDD level of theory on representative model systems. These computations revealed that steric interactions of the CH_3 group on the tri(o-tolyl)phosphine ligand are responsible for the lack of ligand exchange in solution with PPh_3. Our joint experimental and theoretical findings demonstrate the subtle interplay of steric and electronic factors that determine the size distribution, stability, and dissociation pathways of phosphine ligated gold clusters.

INTRODUCTION

Nanoparticles (NPs) and sub-nanometer clusters exhibit novel properties that differ from the bulk making them potentially highly-tunable materials for advanced technological applications. In particular, their potential for applications in catalysis,[1-3] solar energy conversion,[4-6] nanoscale electronics,[7] and biomedicine[8-9] is of great interest. For example, it has been shown that the catalytic activity of gold NPs is related to their size.[10] Specifically, the activity diminishes as the particle size exceeds a diameter of 10 nm,[11-14] demonstrating that size-selected NPs and sub-nanometer clusters play an essential role in catalysis.[15-17] As an adjunct to experiments, many theoretical studies of the catalytic properties of metal nanoclusters have been performed over the past two decades,[18-24] revealing structure-reactivity relationships in the adsorption and activation of key molecules.

Experimentally, NPs and clusters may be prepared with high purity by electron sputtering and evaporation techniques.[25] A viable alternative approach to prepare NPs and clusters involves solution-based reduction of metal salts in the presence of organic ligands. Since such particles have great potential as catalysts and their properties may change substantially with the addition or removal of a single metal atom, it is important to develop synthetic methodologies that are simultaneously controllable, scalable, and reproducible. Therefore, the choice of ligand in solution-based cluster synthesis is crucial to develop an effective catalyst with desired activity, selectivity, and durability. Furthermore, it has been shown both theoretically[20,21, 26-27] and experimentally[28-32] that the use of different ligands during synthesis in solution is central to tailoring the size and properties of the resulting clusters. Ligands such as thiols[33-34] and phosphines[35-37] may be used to direct cluster growth to particular sizes and preserve the cluster distribution formed initially in solution. It follows that in order to develop a comprehensive method for synthesizing clusters with predetermined properties, it is necessary to understand the factors that influence the size and stability of these highly sought-after materials.[38]

Experimentally determining the stability of nanoclusters toward fragmentation of their gold cores and ligand dissociation illuminates the thermodynamics of cluster formation processes in solution and indicates potential applications for clusters of a certain size. While theoretical studies of ligation effects on cluster formation and stability are available in the literature,[39-41] experimental evidence is less readily accessible.[32, 37, 42 43-44] Such experimentally-determined kinetic and thermodynamic parameters are useful for benchmarking the results of high-level theoretical structural calculations and the approximations used therein.[45]

The interactions between organic ligands and metal cores are particularly important in determining the structure and stability of metal nanoclusters.[46] Since the 1970s, phosphine ligands have been employed to control the size of gold nanoclusters during synthesis.[47-49] The size distribution and structures of clusters synthesized using various phosphines have been the subject of ongoing research[50-53] as phosphines may either partially donate charge to the gold core or localize charge within surface gold-phosphine bonds.[39, 54-55] Recent research has focused on understanding the effect of differently-substituted phosphine ligands on cluster synthesis[38] in an effort to determine synthetic procedures and specific ligands that may be useful in the development of a scalable synthetic method for size-selected gold clusters with precisely-defined properties. In this regard, studies have employed mass spectrometry to characterize the fragmentation, stability, and reactivity of gold clusters synthesized with various ligands.[30, 32, 43, 56-63] Because gold clusters have been successfully studied using both theoretical and experimental methods,[64-66] we expect that the combined approach used herein will enable a clearer understanding of the experimental results. For example, a previous experimental and computational study examined the catalytic activity of Au_3 nanoclusters in organometallic synthesis.[65, 67] In addition to demonstrating the importance of gas-phase ion chemistry to understanding catalytic processes, this previous study highlighted the importance of the type of ligand on these clusters in affecting catalytic activity. Another theoretical[64] work examined ligand effects on the electronic structure of $M_3L_3^+$ nanoclusters (M = Cu, Ag, Au; L = CO). They concluded that CO binding increased the aromaticity of the gold core on the $Au_3L_3^+$ clusters. In addition, they found that electrostatic contributions to the M-L bond are more prominent than their covalent counterpart.

In this contribution, we describe the influence of steric changes to phosphines ligands on the extent of ligand exchange reactions, final cluster size distributions, and cluster stability by systematically exchanging three different tri(tolyl)phosphine ligands onto preformed gold clusters ligated with PPh_3. The tri(tolyl)phosphine ligands with methyl groups located at the meta and para positions of the phenyl rings are shown to readily exchange with PPh_3 ligands on the preformed gold clusters. In comparison, the tri(ortho-tolyl)phosphine ligands do not exchange onto the nascent cluster distribution leaving the PPh_3-ligated clusters intact. Of the different size species in the cluster distribution, the $Au_8L_7^{2+}$ clusters were most abundant and, therefore, were selected for further study by collision-induced dissociation. In general, the mixed-ligand clusters containing both PPh_3 and tri(tolyl)phosphine ligands were found to dissociate through loss of PPh_3, suggesting that the tri(tolyl)phosphine ligands interact more strongly with the gold cores than PPh_3. To examine in greater detail the factors affecting the electronic structure of these clusters we also performed quantum mechanical computations using a representative gold-ligand complex, AuL^+, and three-atom gold cluster with its corresponding ligands, $Au_3L_3^+$, where L = PPh_3, TOTP, TMTP and TPTP. Collectively, our joint experimental and theoretical findings show that functional groups located beyond the primary phosphine coordinating centers of the ligands influence cluster size and stability through both electronic and steric factors.

EXPERIMENTAL METHODS

Cluster Synthesis

All chemicals were used without further purification. The chloro(triphenylphosphine)gold(I) (99.9%, $AuPPh_3Cl$, CAS: 14243-64-2) and chloro[tri(o-tolyl)phosphine)gold(I) (95%, Au(TOTP)Cl, CAS: 83076-07-7) precursors and borane *tert*-butylamine (97%, BTBA, CAS: 7337-45-3) reducing agent were purchased from Sigma-Aldrich (St. Louis, MO), and methanol (99.8%, CAS: 67-56-1) was obtained from Fisher Scientific (Hampton, NH). The triphenylphosphine (99%, PPh_3, CAS: 603-35-0), tri(p-tolyl)phosphine (TPTP, CAS: 1038-95-5), and tri(o-tolyl)phosphine (TOTP, CAS: 6163-58-2) ligands were also obtained from Sigma Aldrich. The tri(m-tolyl)phosphine (TMTP, CAS: 6224-63-1) ligand was obtained from Acros Organics (Tokyo, Japan).

The batch synthesis of monodentate phosphine-ligated gold clusters followed procedures previously reported in the literature.[42, 68] Briefly, the $AuPPh_3Cl$ gold precursor was dissolved in methanol to prepare a 500 μM stock solution. The BTBA reducing agent was dissolved in methanol to prepare a 50 mM stock solution. Note that the ligand stock solutions (1 mM in Ar-purged methanol) were prepared daily to avoid degradation and oxidation that occurs with prolonged exposure to air. The gold ($AuPPh_3Cl$ or Au(TOTP)Cl) precursor and BTBA stock solutions were combined in a 1.5 mL plastic microcentrifuge tube with methanol to prepare a 0.1 mM gold precursor and 5 mM reducing agent solution, which was mixed for 1–2 min on a vortexer to initiate formation of the PPh_3-ligated gold clusters [*i.e.,* ($Au_6L_6Cl_2$), ($Au_7L_6Cl_2$), ($Au_8L_7Cl_2$), ($Au_9L_7Cl_2$) and ($Au_9L_8Cl_2$)]. To initiate ligand exchange, one of three tolyl-ligand solutions was added to the fresh PPh_3-ligated gold cluster solution and mixed. Following mixing, the solutions were immediately analyzed by electrospray ionization mass spectrometry (ESI-MS) in the positive ion mode.

Mass Spectrometry

ESI-MS spectra were obtained using a Bruker HCT Ultra ion trap instrument (Bruker Daltonics, Bremen, Germany). The HCT Ultra instrument was operated in a mass range of $m/z = 200 – 3000$. In positive ion mode the source conditions employed were as follows: capillary voltage of 3200 V, drying gas (N_2) flow rate of 5 L min^{-1}, and drying gas temperature of 200 ºC. In order to avoid the possibility of tolyl ligand cross contamination between experiments the commercial electrospray lines and nebulizer unit were not used. Instead, homemade electrospray lines (150 μm outer diameter / 50 μm inner diameter, Polymicro Technologies) were used as ESI emitters along with cleaned glass syringes (500 μL Hamilton) for each different tri(tolyl)phosphine ligand. Typical settings for the ion optics were as follows: skimmer, 75 V; capillary exit, 95 V; Oct 1, DC 16 V; Oct 2, DC 0 V; trap drive, 150; Oct RF, 50 $V_{p\text{-}p}$; lens 1, 14 V; and lens 2, 32 V. Tandem mass spectrometry (MS/MS) experiments were performed with the HCT Ultra instrument using a primary ion isolation window of *m/z* = 4 and helium as the collision gas in the auto MS^n configuration with the default mass cutoff of 27%. The total ion abundance was similar between different spectra. The potential gradient in the high-pressure source region of the instrument was minimized and the temperature of the heated capillary was lowered to avoid collisional fragmentation or thermal degradation of the nascent ions from solution. Molecular formulas of the clusters were assigned on the basis of *m/z*, the charge-state dependent separation of individual peaks making up each peak envelope, and the overall match of the isotopic distributions with those calculated using a molecular weight calculator program (see https://omics.pnl.gov/software/molecular-weight-calculator).

Theoretical Methods

Quantum mechanical computations were performed using the Gaussian 09 suite of programs.[69] The density functional theory (DFT) method based on Becke's three-parameter functional with the Lee, Yang, and Parr correlation[70-72] with empirical dispersion (B3LYP-D3) in combination with the SDD[73] basis set were employed for ground-state geometry optimizations. Frequency calculations performed on the optimized geometries of all the complexes and the three-atom gold clusters confirmed that each structure was a local minimum. In addition, we performed a natural bond orbital (NBO) analysis[74] on all of the optimized structures in order to investigate non-bonding interactions.

RESULTS AND DISCUSSION

A graphical representation of the ligand exchange process for a representative three-atom gold cluster containing three ligands is shown in **Scheme 1**. The three numbers in parentheses are used to specify the number of gold atoms, PPh_3 ligands, and exchanged tri(tolyl)phosphine ligands, respectively. The charge state of the clusters is shown as a superscript on the upper right of the parentheses. A gold cluster containing three native PPh_3 ligands without any exchange, which in our nomenclature is $(3,3,0)^+$, is presented in the top left corner of **Scheme 1.** Moving counterclockwise, the product of the first ligand exchange is $(3,2,1)^+$, where one of the PPh_3 ligands has been exchanged for a TPTP ligand. Next, a second exchange of PPh_3 with TPTP results in the formation of the $(3,1,2)^+$ cluster in the lower right corner. Finally, the $(3,0,3)^+$ cluster, which represents complete exchange of all PPh_3 ligands with TPTP, is shown in the top right corner of **Scheme 1.** Each ligand-exchanged cluster gives rise to a distinct pattern of peaks in the mass spectrum of the cluster solution. For the representative example shown in **Scheme 1**, four peaks 42 *m/z* apart from each other are expected in the mass spectrum. For a doubly charged cluster, the peak separation due to the additional CH_3 groups of the tri(tolyl)phosphine ligands (three per exchanged ligand in place of the original hydrogen atoms) will be 21 mass units because of the second charge.

To explore the influence of differently substituted phosphine ligands on the nascent size distribution and fragmentation behavior of $Au_8L_7^{2+}$ (L = PPh_3) clusters the position of the methyl group in the exchanged tri(tolyl)phosphine ligands was systematically varied (-ortho, -meta, -para) and the resultant effects on cluster size, charge distribution, and fragmentation were characterized by ESI-MS. Full range mass spectra obtained from these experiments are available as supplementary information in Figure S1. A representative mass spectrum (1200 to 2200 *m/z*) of the preformed PPh_3-ligated gold nanoclusters is presented in **Figure 1a**. Several clusters were observed ranging in size from six to nine gold atoms, with clusters containing eight gold atoms exhibiting the highest abundance. No new peaks were observed in the mass spectrum when TOTP was introduced for ligand exchange (**Figure 1(b)**). Notably, ligand exchange with gold nanoclusters preformed with PPh_3 occurred only for TMTP and TPTP ligands (**Figures 1(c)–(d)**). As a consequence of ligand exchange reactions, seven new peaks corresponding to different *m/z* were observed in **Figure 1(c)-(d)**. The remaining high abundance of the $(8,7,0)^{2+}$ cluster suggests that while tolyl ligands may have the ability to stabilize clusters electronically, steric hindrance may limit the total number of ligands that bind to the gold core. Closer examination of Figure 1(b) reveals that the abundance of the PPh_3-ligated gold nanoclusters was lower than the precursor solution in Figure 1(a). To gain a better understanding of this phenomenon we performed time-dependent experiments over the course of 48 hrs on the PPh_3/TOTP ligand exchange synthesis shown in Figure 1(b) (Figure S2). The abundance of the cluster peaks was lower due to (major) ligand oxidation (279, 352 *m/z*) after 48 hrs. We also ligand exchanged PPh_3 onto preformed TMTP ligated clusters (**Figure S3**). In this case, no change in the size, abundance, or distribution of the TMTP-ligated clusters was evident over a 24 hr period, suggesting that these clusters are stable once they are formed.

In order to better understand the experimental findings, an NBO steric analysis[74] was performed on representative AuL^+ complex and $Au_3L_3^+$ cluster geometries optimized using DFT. A plot of the total interaction energies calculated for all four AuL^+ complexes is provided in **Figure 2**. The TOTP ligand in the AuL^+ complex generates the largest steric interaction of all the tri(tolyl)phosphine ligands. Although different types of interactions are associated with these gold-ligand complexes, the steric interactions of the ligands with the gold atoms appear to play a substantial role in determining whether or not ligand exchange is energetically favorable. Indeed, all complexes show strong steric interactions between gold atoms and ligands of the type $\sigma_{(P\text{-}C)} \rightarrow \sigma_{(Au\text{-}P)}$ and $\sigma_{(C\text{-}C)} \rightarrow \sigma_{(Au\text{-}P)}$. Moreover, for the complex containing TOTP, there is an additional interaction ($\sigma_{(C\text{-}H)} \rightarrow \sigma_{(Au\text{-}P)}$, insert **Figure 2a**) caused by the close proximity of the CH_3 group to gold atom. As expected, the CH_3 group in the ortho position of the ligand creates an additional steric interaction compared to the meta and para positions. To explore the electronic effect of the CH_3 group on the phosphine ligand, NBO charges on the phosphorus and gold atoms were calculated. Although the charges are different for all the complexes (Figure S4), the $\sigma_{(Au\text{-}P)}$ bond distances within $Au(PPh_3)^+$, $Au(TPTP)^+$, and $Au(TMTP)^+$ complexes are unaffected, as evidenced by their respective distances of 2.364, 2.364, and 2.366 Å. In contrast, the $Au(TOTP)^+$ complex has a $\sigma_{(Au\text{-}P)}$ bond distance of 2.380 Å. This confirms that the steric effects of the o-tolyl group play a key role on the structure of these complexes. Moreover, the $\sigma_{(C\text{-}H)} \rightarrow \pi_{(C\text{-}C)}$ (insert Fig. 2b) steric interaction is present only in the Au-TOTP complex. We postulated that the steric interactions shown in **Figure 2** increase as the number of gold atoms in the cluster core increases. Moreover, we hypothesized that the principal reason that the TOTP ligand does not participate in ligand exchange reactions is because of the $\sigma_{(C\text{-}H)}$ bond interacting with the gold cluster. To test this hypothesis, representative three-atom gold clusters containing three ligands, $Au_3L_3^+$, where L is PPh_3, TPTP, TMTP or TOTP, were optimized at the B3LYP-D3/SDD level of theory and an NBO analysis was performed. The gold cluster structures with the PPh_3, TPTP, TMTP and TOTP ligands are shown in **Figure S5**. The corresponding average steric interaction energies between each of the ligands and the gold core are calculated to be 130, 128, and 139 kJ mol^{-1} for PPh_3, TPTP, and TMTP, respectively (**Table S1**). In comparison, the average steric interaction energy of the cluster containing the TOTP ligand, shown in **Figure 3**, is 159 kJ mol^{-1}. This trend in the steric interaction energies is similar to the one observed for the AuL^+ complexes where the TOTP ligand has the highest steric energy relative to PPh_3, TPTP, and TMTP (**see Figure 2a**). As predicted, these representative $Au_3L_3^+$ clusters exhibit the same types of interactions as the AuL^+ complexes. In addition, a new type of interaction emerges ($\sigma_{(C\text{-}H)} \rightarrow \sigma_{(Au\text{-}Au)}$) following formation of the gold-gold bond, which is shown as a contour plot in **Figure 3a**. Similar to the AuTOTP complex, the tolyl-CH_3 also results in a ligand-ligand steric interaction in the $Au_3L_3^+$ cluster. A contour plot of the $\sigma_{(C\text{-}H)} \rightarrow \pi_{(C\text{-}C)}$ interaction is shown in **Figure 3b**. This particular interaction is present in all of the tolyl-substituted clusters investigated herein. As the ligands enter into close proximity, another interaction that arises is the $\sigma_{(C\text{-}H)} \rightarrow \sigma_{(C\text{-}H)}$ of the tolyl groups. This interaction is the largest in the $Au_3(TMTP)_3^+$ cluster and the least in $Au_3(TOTP)_3^+$. As shown in Table S1, the average steric energy for the tolyl-substituted gold clusters is 31, 40, and 36 kJ mol^{-1} for the $Au_3(TOTP)_3^+$,

$Au_3(TMTP)_3^+$, and $Au_3(TPTP)_3^+$ clusters, respectively. The primary reason for this is the meta position of the CH_3-tolyl group which maximizes $\sigma_{(C\text{-}H)} \rightarrow \sigma_{(C\text{-}H)}$ interactions. As expected, the $Au_3(PPh_3)_3^+$ cluster has the lowest ligand-ligand steric interaction energy, with an average value of 28 kJ mol^{-1}. Another important observation is that the gold-gold bond of all three sides of the $Au_3(TOTP)_3^+$ cluster are within 0.01 Å of each other whereas the other TMTP and TPTP clusters have two identical sides and one that is shorter (by 0.04 Å). This structural difference is evident in the ligand-ligand interaction. In Table 1, the average L1 → L3 steric energy is around 8 kJ mol^{-1} for PPh_3, TMTP, and TPTP and 28 kJ mol^{-1} for TOTP. In contrast, the interactions between L1 → L2 and L2 → L3 are substantially larger. Meanwhile, the TOTP ligands have similar energy values for all three ligand-ligand interactions. Despite these values the ligand-ligand interaction energies of these clusters are four times smaller than the interactions between the ligands and the Au_3 core. Therefore, based on these results, we hypothesized that the interaction between the ligand and the gold core is the predominant one that has to be overcome during ligand exchange reactions. Furthermore, since our theoretical analysis shows that the TOTP ligand has the highest ligand-gold interaction, we conclude that ligand exchange between PPh_3 and TOTP ligands is the least favorable of the tolyl-phosphines reported herein. To provide evidence supporting this statement we performed additional time-dependent experiments where the alternate Au(TOTP)Cl gold precursor complex was reacted with BTBA instead of $Au(PPh_3)Cl$ in an attempt to form clusters without PPh_3. This attempted synthesis resulted in the formation of only AuL_2^+ (L = TOTP) for the sterically hindered TOTP ligand (**Figure S6**). These experimental (**Figure 1**, **Figure S6**) and theoretical (**Figure 3, Table 1**) findings suggest that steric interactions in tolyl-phosphine ligated gold clusters largely govern their structures and size distributions.

Although $(8,7,0)^{2+}$ is relatively abundant in all of the cluster syntheses, it undergoes ligand exchange reactions with only the meta- and para-substituted tri(tolyl)phosphine ligands investigated herein. Due to steric hindrance, the ortho-substituted tolyl ligand does not participate in ligand exchange reactions on this cluster. Therefore, due to their large abundance and reactivity toward ligand exchange the $(8,x,y)^{2+}$ gold clusters were selected for energy-dependent fragmentation experiments. Specifically, the clusters were mass selected for collision-induced dissociation (CID) experiments to observe their relative stability toward fragmentation in the gas phase. MS^2 experiments were also performed in which the amplitude of excitation was systematically varied, resulting in twenty one individual CID experiments. After varying the amplitude of excitation in each experiment, the abundance of each fragment ion was used to calculate the percent fragmentation at amplitudes corresponding to 40–60% of the parent ion fragmentation.

A plot of the percent parent ion fragmentation and product ion yield versus the amplitude of excitation for $(8,7)^{2+}$ is shown in **Figure 4**. Five major product ion peaks were produced as a consequence of the CID experiments, corresponding to eight- and seven-atom gold clusters, as well as a one-gold atom two-ligand complex. The loss of one PPh_3 ligand to produce $(8,6)^{2+}$ is plotted as the open circles in **Figure 4**. Notably, there was a ~4% product ion yield at an excitation amplitude of only 0.1, which remained constant until an amplitude of 0.6 was reached. This may be due to some residual in-source fragmentation. At amplitudes higher than 0.6, the product ion percentage of $(8,6)^{2+}$ increased and reached a maximum of 20% at 0.8 amplitude. For all of the other product clusters and the one-gold atom complex, fragmentation began at an excitation amplitude of 0.6. After removal of two ligands the $(8,7)^{2+}$ clusters lost a gold atom and an additional ligand in an asymmetric fragmentation process giving rise to $(7,4)^{+}$ (dashed line, **Figure 4**). Simultaneously, a $(7,3)^{+}$ product ion appeared, which corresponds to the loss of a gold atom and four ligands (solid line, **Figure 4**), likely through a secondary fragmentation pathway, while also giving rise to $(1,2)^{+}$ (solid line/solid triangles, **Figure 4**). At 33.8%, the $Au(PPh_3)_2^+$ product ion complex had the highest abundance of any fragmentation product at high excitation amplitudes. Notably, these CID results confirm the relatively high stability of the eight- and seven-atom gold clusters. In order to investigate the effect of ligand exchange on the stability of these clusters, these results for PPh_3-ligated $(8,7)^{2+}$ were compared with those of CID experiments on mixed-phosphine clusters containing tolyl groups. As noted above, TOTP does not participate in ligand exchange reactions so only clusters containing TMTP and TPTP ligands were analyzed by CID. First, we explore ligand exchange of TMTP onto preformed PPh_3-ligated gold clusters. Two superimposed mass spectra that cover the mass range for doubly charged eight-atom gold clusters are shown in **Figure 5**, illustrating the distribution of clusters before and after ligand exchange with TMTP.

As a consequence of ligand exchange reactions, seven new peaks are observed in the mass spectrum. A balanced distribution of mixed-ligand clusters is present, with the $(8,5,2)^{2+}$, $(8,4,3)^{2+}$, and $(8,3,4)^{2+}$ clusters having the highest relative abundance. The highest abundance peak overall, corresponding to $(8,7,0)^{2+}$ in **Figure 5**, results from no ligand exchange with TMTP. We performed CID experiments on each of the mixed-ligand clusters shown in **Figure 5**. For each ligand-exchanged cluster, the MS^2 experiments yielded seven- and eight-atom gold clusters and one-gold atom two-ligand complexes. Therefore, each peak shown in **Figure 5** produces a spectrum of CID products similar to that shown in **Figure 4** for $(8,7,0)^{2+}$ (**Figures S7–S13**). The percent dissociation at similar energies is higher for PPh_3 than TMTP for almost all the mixed-ligand clusters except $(8,1,6)^{2+}$. This result implies that the TMTP ligand may be better at stabilizing eight-atom gold clusters than PPh_3.

Compared to PPh_3, TPTP has similar interactions and comparable fragmentation results, therefore, are expected. When the mass spectrum resulting from ligand exchange of PPh_3 with TPTP was analyzed, it was apparent that TPTP undergoes full exchange with all of the seven PPh_3 ligands in the $(8,7,0)^{2+}$ cluster (**Figure 6**). Similar to the results for TMTP exchange, a Gaussian-like distribution of the TPTP exchanged clusters was observed, with $(8,4,3)^{2+}$ and $(8,3,4)^{2+}$ exhibiting the highest relative abundances of the mixed ligand clusters.

CID experiments were also performed on each of the TPTP exchanged clusters shown in **Figure 6**. For each mixed ligand cluster, plots of the percent fragmentation versus the amplitude of excitation are given in **Figures S14–S19** of the Supplementary Information. The data shows the formation of eight- and seven-atom cluster fragments and one-gold atom two-ligand complexes for each TPTP-containing cluster, similar to the CID results observed with PPh_3- and TMTP-containing clusters. Regardless of the number of ligands exchanged, the dissociation of the clusters initiated at amplitudes of excitation between 0.7 and 0.8. The unexchanged $(8,7,0)^{2+}$ cluster also fragmented at amplitudes of 0.7–0.8, indicating that the less-TPTP exchanged clusters have similar stability to the unexchanged PPh_3-containing clusters. The fully TPTP-exchanged cluster, which fragments at ~0.58 amplitude, was found to be an exception that indicates the relative instability of a completely TPTP-ligated cluster. This difference in stability may be caused by electronic effects of the methyl group substitution as steric contributions should be minimal with methyl substitution in the para position of the phenyl rings.

Previous experiments that examined the relative stability of gold clusters ligated with different phosphines showed that the calculated proton affinities of the phosphines correlate with the fractional abundance of their fragmentation yield.[42] To compare the CID data obtained in this work to the previously published results for methyl- and cyclohexyl-substituted phosphines the fractional abundance of PPh_3 fragmentation in the TMTP, TPTP, and PPh_3 mixed-ligand clusters was calculated using Equation 1:

$$Fractional\ Abundance\ of\ PPh_3 = \frac{I(PPh_3)/N(PPh_3)}{I(PPh_3)/N(PPh_3)+I(L)/N(L)} \tag{1}$$

where I is the ion abundance, N is the number of ligands present on the mixed ligand cluster, and L refers to either TMTP or TPTP. Fractional abundances calculated in this way compare the relative binding energies of any exchanged ligand to PPh_3. A comparison of the relative fragmentation yields of PPh_3 and the two tolylphosphine exchange ligands is given in **Figure 7**. Both TMTP and TPTP bind more strongly to the gold core than PPh_3 as the fractional abundance of PPh_3 is greater than 50 % for all of the mixed-ligand clusters studied herein. These results are in agreement with previous findings that suggest that the proton affinity values calculated in the Ligand Knowledge Base[54] show a direct correlation with the experimentally determined relative ligand binding energies for all phosphine ligands studied on a single Au_8^{2+} gold core.

CONCLUSIONS

We present experimental and theoretical evidence that steric factors play an important role in governing the synthesis, stability, and activity of phosphine-ligated gold clusters. We show that the TOTP ligand does not undergo ligand exchange with PPh_3 on preformed gold clusters due to unfavorable steric interactions between the $\sigma_{(C\text{-}H)}$ bond of the CH_3 functional group and the $\sigma_{(Au\text{-}Au)}$ and $\sigma_{(P\text{-}Au)}$ bonds. In contrast, the TMTP and TPTP ligands are demonstrated to be better at stabilizing gold clusters than the PPh_3 ligand, as evidenced by their extensive ligand exchange and relatively stronger binding to the core. Finally, the yield of the PPh_3 fragments is shown to be influenced by both cluster size and the position of the methyl group in the tolyl ligands of the gold clusters. Our results provide insight into how steric factors in phosphine ligands may be leveraged alongside an emerging understanding of electronic structure to rationally prepare scalable quantities of clusters of predetermined size and stability for a range of technological applications.

CONFLICTS OF INTEREST

The authors declare no conflict of interest.

ACKNOWLEDGEMENTS

This work was supported in part by the U.S. Department of Energy, Office of Science, and Office of Workforce Development for Teachers and Scientist (WDTS) under the Visiting Faculty Program (VFP). It was also partially supported by the U.S. Department of Energy, Office of Science, and Office of Basic Energy Sciences, Division of Chemical Sciences, Geosciences and Biosciences. KP and MK acknowledge support from the DOE Science Undergraduate Laboratory Internship (SULI) program. This work was performed using EMSL, a national scientific user facility sponsored by the DOE's Office of Biological and Environmental Research and located at Pacific Northwest National Laboratory (PNNL). PNNL is a multiprogram national laboratory operated for DOE by Battelle.

Figures and Tables

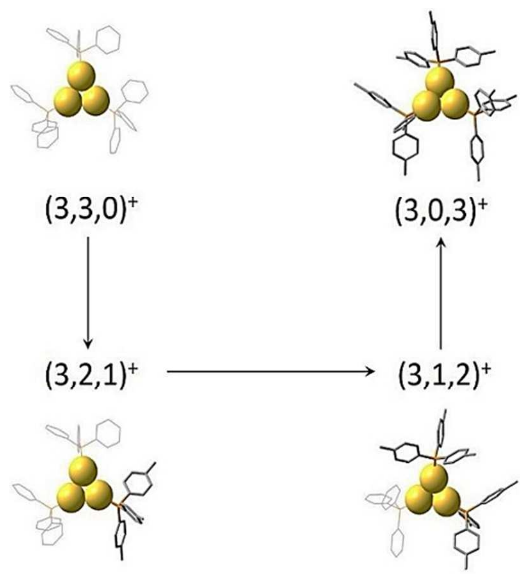

Scheme 1. Graphical representation of the ligand exchange process for a representative three atom gold cluster containing three ligands.

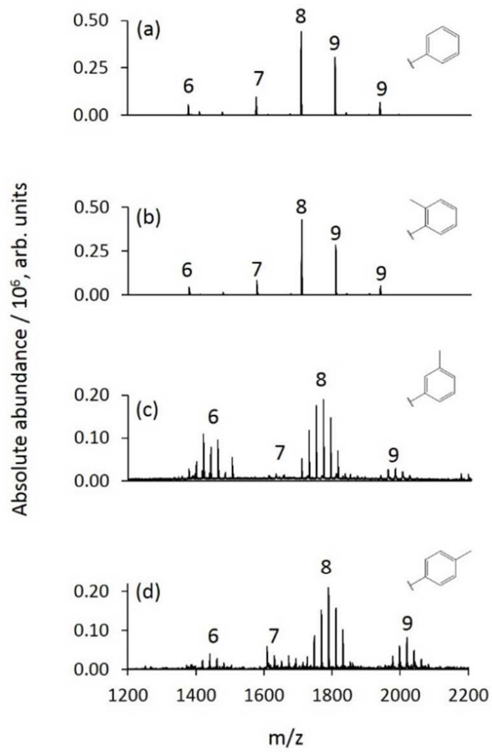

Fig. 1. Representative positive mode ESI-MS spectra of the (a) nascent gold clusters with PPh_3 ligands, (b) after addition of TOTP showing no ligand exchange or etching (see Figure S1 for full mass range spectru,), (c) TMTP and (d) TPTP. The numbers indicate the quantity of gold atoms in each group of clusters. Note: of the two 9 gold atom peaks, one includes 7 ligands and the other includes 8 ligands.

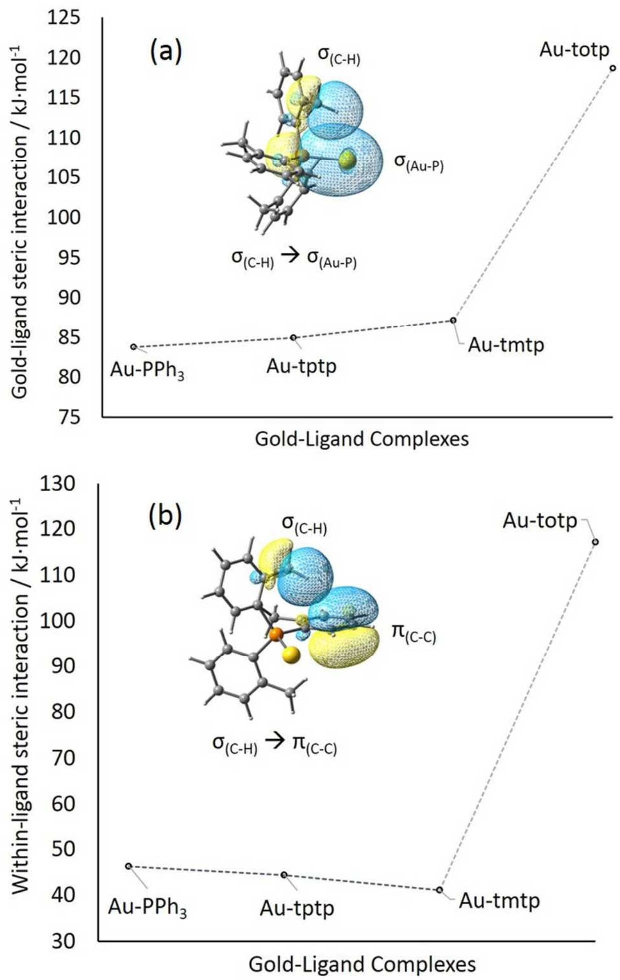

Fig. 2. Plot of the calculated steric interaction energies (B3LYP-D3/SDD) as a function of the position of CH_3 substitution in the phenyl rings using natural bond orbital steric analysis of the tolyl-gold complexes (Au-L). The steric energy is the sum of all the steric interactions (a) between gold and the tolyl ligands, and (b) within ligand interaction. The $\sigma_{(C\text{-}H)} \rightarrow \sigma_{(Au\text{-}P)}$ (insert Fig. 2a) and the $\sigma_{(C\text{-}H)} \rightarrow \pi_{(C\text{-}C)}$ (insert Fig. 2b) steric interactions are present only in the Au-TOTP complex.

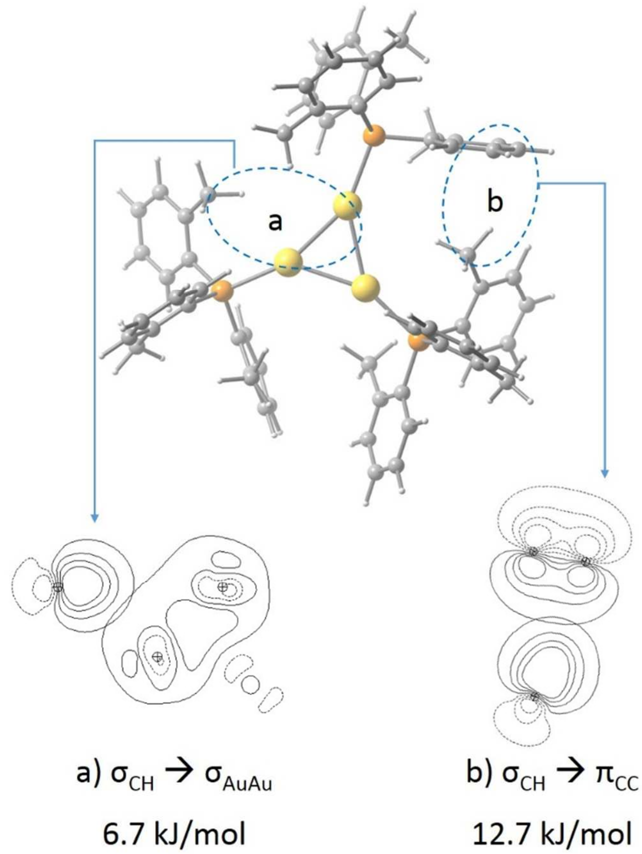

Fig. 3. Optimized structures of the $Au_3(TOTP)_3^+$ cluster at the B3LYP-D3/SDD level of theory. The $\sigma_{(C\text{-}H)}$ orbital of the tolyl-CH_3 group elicits a large steric interaction. (a) A $\sigma_{(C\text{-}H)} \rightarrow \sigma_{(Au\text{-}P)}$ due to the interaction of the ligands with the gold core and (b) a $\sigma_{(C\text{-}H)} \rightarrow \pi_{(C\text{-}C)}$ interaction due to interaction between ligands. For clarity, only one $\sigma_{(C\text{-}H)} \rightarrow \sigma_{(Au\text{-}Au)}$ and one $\sigma_{(C\text{-}H)} \rightarrow \pi_{(C\text{-}C)}$ interaction are shown. Note that the CH_3 group in the third ligand is directed away from the gold core.

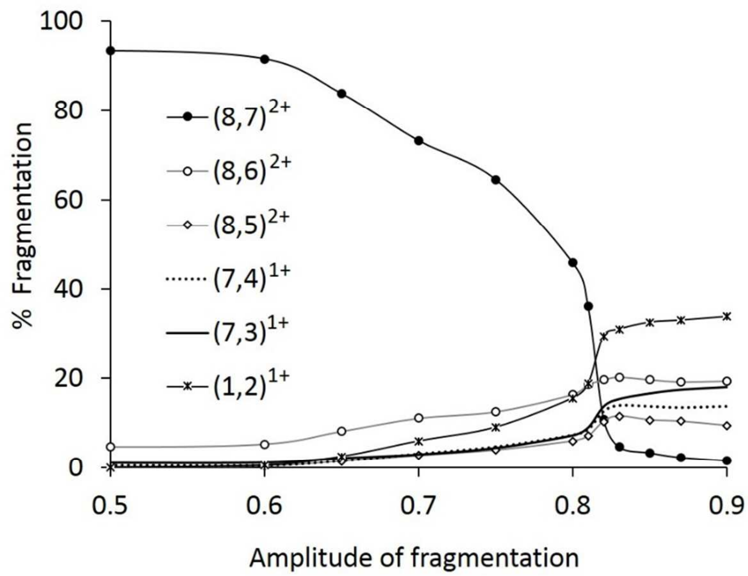

Fig. 4. Collision-induced dissociation data for the $(8,7)^{2+}$ gold cluster. Twenty-one experiments were performed where the amplitude of fragmentation was varied in units of 0.05 from 0.1 to 0.8 and in units of 0.02 from 0.8 to 0.9.

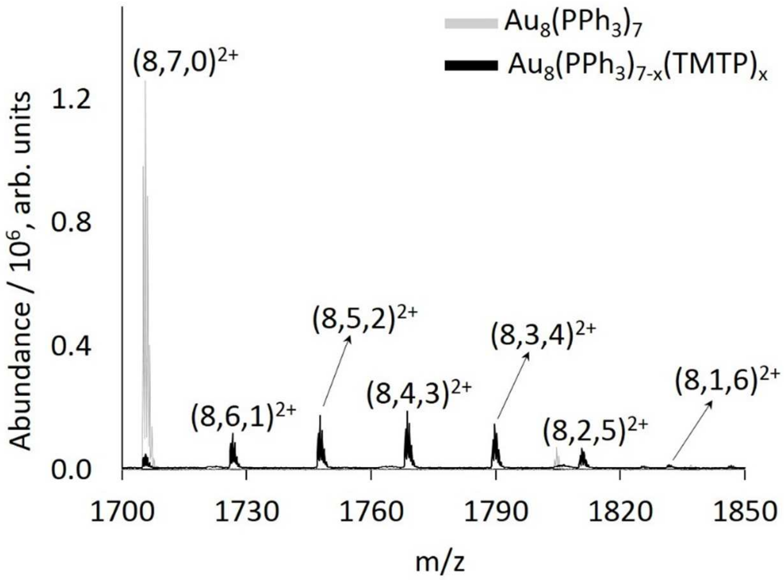

Fig. 5. Superimposed mass spectra of the $[Au_8(PPh_3)_7]^{2+}$ cluster (gray, highest abundance peak) and a series of $Au_8(PPh_3)_{7-x}(TMTP)_x$ ($x = 0 - 6$) mixed ligand clusters (black peaks).

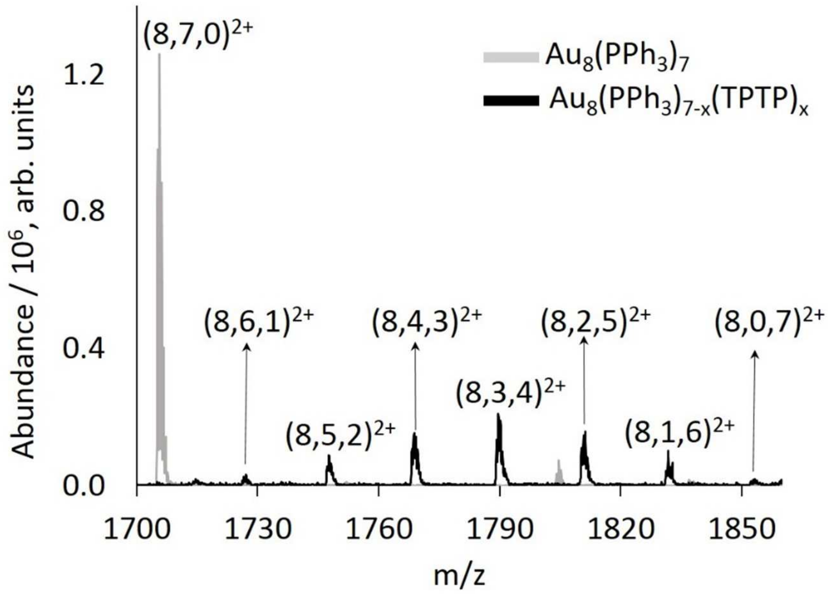

Fig. 6. Mass spectrum of a series of $Au_8(PPh_3)_{7-x}(TPTP)_x$ (x = 0 – 7) mixed-ligand clusters (black peaks).

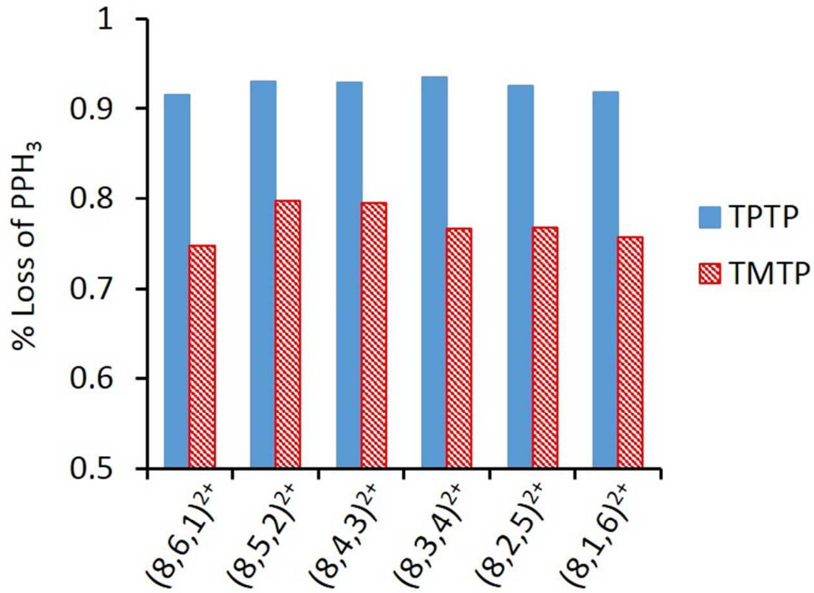

Fig. 7. Chart showing the relative CID fragmentation yields of PPh_3 *vs.* TMTP and TPTP for all of the ligand exchanged clusters. The percent loss of PPh_3 is calculated as a relative percent using equation 1.

Table 1. Calculated values from NBO analysis of the steric interactions between individual ligands and gold atoms in the $(3,3)^+$ cluster.

	Steric interaction / $kJ\cdot mol^{-1}$					
Ligand (L)	L1 → Au_3	L2 → Au_3	L3 → Au_3	L1 → L2	L1 → L3	L2 → L3
PPh_3	129.7	117.4	141.7	54.0	8.5	22.0
TPTP	140.5	115.7	127.7	32.9	7.2	69.2
TMTP	135.5	126.4	153.8	84.9	9.2	24.6
TOTP	176.4	140.4	161.2	27.9	28.0	36.6

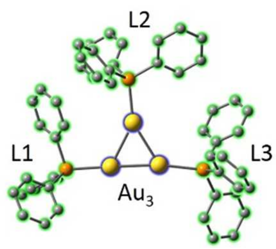

Scheme 2. A three dimensional 3D rendering of the $Au_3L_3^+$ cluster to accompany **Table 1**.

REFERENCES

1. Haruta, M., Size- and support-dependency in the catalysis of gold. *Catal Today* **1997,** *36* (1), 153-166.
2. Yamazoe, S.; Koyasu, K.; Tsukuda, T., Nonscalable Oxidation Catalysis of Gold Clusters. *Accounts Chem Res* **2014,** *47* (3), 816-824.
3. Zhu, Y.; Qian, H. F.; Jin, R. C., Catalysis opportunities of atomically precise gold nanoclusters. *J Mater Chem* **2011,** *21* (19), 6793-6799.
4. Westphalen, M.; Kreibig, U.; Rostalski, J.; Luth, H.; Meissner, D., Metal cluster enhanced organic solar cells. *Sol Energ Mat Sol C* **2000,** *61* (1), 97-105.
5. Stenzel, O.; Wilbrandt, S.; Stendal, A.; Beckers, U.; Voigtsberger, K.; Vonborczyskowski, C., The Incorporation of Metal-Clusters into Thin Organic-Dye Layers as a Method for Producing Strongly Absorbing Composite Layers - an Oscillator Model Approach to Resonant Metal Cluster Absorption. *J Phys D Appl Phys* **1995,** *28* (10), 2154-2162.
6. Chen, Y. S.; Choi, H.; Kamat, P. V., Metal-Cluster-Sensitized Solar Cells. A New Class of Thiolated Gold Sensitizers Delivering Efficiency Greater Than 2%. *J. Am. Chem. Soc.* **2013,** *135* (24), 8822-8825.
7. Ko, S. H.; Park, I.; Pan, H.; Grigoropoulos, C. P.; Pisano, A. P.; Luscombe, C. K.; Frechet, J. M. J., Direct nanoimprinting of metal nanoparticles for nanoscale electronics fabrication. *Nano Lett* **2007,** *7* (7), 1869-1877.
8. Cai, W.; Gao, T.; Hong, H.; Sun, J., Applications of gold nanoparticles in cancer nanotechnology. *Nanotechnol Sci Appl* **2008,** *1*, 17-32.
9. Jain, P. K.; Lee, K. S.; El-Sayed, I. H.; El-Sayed, M. A., Calculated absorption and scattering properties of gold nanoparticles of different size, shape, and composition: Applications in biological imaging and biomedicine. *J Phys Chem B* **2006,** *110* (14), 7238-7248.
10. Corma, A.; Garcia, H., Supported gold nanoparticles as catalysts for organic reactions. *Chem Soc Rev* **2008,** *37* (9), 2096-2126.
11. Castano, M. G.; Reina, T. R.; Ivanova, S.; Centeno, M. A.; Odriozola, J. A., Pt vs. Au in water-gas shift reaction. *J Catal* **2014,** *314*, 1-9.
12. Nikolaev, S. A.; Permyakov, N. A.; Smirnov, V. V.; Vasil'kov, A. Y.; Lanin, S. N., Selective hydrogenation of phenylacetylene into styrene on gold nanoparticles. *Kinet Catal+* **2010,** *51* (2), 288-292.
13. Gomez-Quero, S.; Cardenas-Lizana, F.; Keane, M. A., Unique selectivity in the hydrodechlorination of 2,4-dichlorophenol over hematite-supported Au. *J Catal* **2013,** *303*, 41-49.
14. Cardenas-Lizana, F.; Keane, M. A., The development of gold catalysts for use in hydrogenation reactions. *J Mater Sci* **2013,** *48* (2), 543-564.
15. Vajda, S.; White, M. G., Catalysis Applications of Size-Selected Cluster Deposition. *Acs Catal* **2015,** *5* (12), 7152-7176.
16. Herzing, A. A.; Kiely, C. J.; Carley, A. F.; Landon, P.; Hutchings, G. J., Identification of Active Gold Nanoclusters on Iron Oxide Supports for CO Oxidation. *Science* **2008,** *321*, 1331-1335.
17. Turner, M.; Golovko, V. B.; Vaughan, O. P. H.; Abdulkin, P.; Berenguer-Murcia, A.; Tikhov, M. S.; Johnson, B. F. G.; Lambert, R. M., Selective oxidation with dioxygen by gold nanoparticle catalysts derived from 55-atom clusters. *Nature* **2008,** *454*, 981-983.
18. Davran-Candan, T.; Gunay, M. E.; Yildirim, R., Structure and activity relationship for CO and O-2 adsorption over gold nanoparticles using density functional theory and artificial neural networks. *J Chem Phys* **2010,** *132* (17).
19. Staykov, A.; Nishimi, T.; Yoshizawa, K.; Ishihara, T., Oxygen Activation on Nanometer-Size Gold Nanoparticles. *J Phys Chem C* **2012,** *116* (30), 15992-16000.
20. Goel, S.; Velizhanin, K. A.; Piryatinski, A.; Tretiak, S.; Ivanov, S. A., DFT Study of Ligand Binding to Small Gold Clusters. *J Phys Chem Lett* **2010,** *1* (6), 927-931.
21. Lyalin, A.; Taketsugu, T., Cooperative Adsorption of O-2 and C2H4 on Small Gold Clusters. *J Phys Chem C* **2009,** *113* (30), 12930-12934.
22. Jimenez-Izal, E.; Alexandrova, A. N., Computational Design of Clusters for Catalysis. *Annual Review of Physical Chemistry* **2018,** *69*, 377-400.
23. Wang, Y.-G.; Mei, D.; Glezakou, V.-A.; Li, J.; Rousseau, R., Dynamic formation of single-atom catalytic active sites on ceria-supported gold nanoparticles. *Nature Communications* **2015,** *6*, 6511(1-8).
24. Wu, Z.; Hu, G.; Jiang, D.-e.; Mullins, D. R.; Zhang, Q.-F.; Allard, J., Lawrence F. ; Wang, L.-S.; Overbury, S. H., Diphosphine-Protected Au22 Nanoclusters on Oxide Supports Are Active for Gas-Phase Catalysis without Ligand Removal. *Nano Lett* **2016,** *16*, 6560-6567.
25. Wender, H.; Migowski, P.; Feil, A. F.; Texeira, S. R.; Dupont, J., Sputeposition of nanoparticles onto liquid substrates: Recent advances and future trends. *Coordination Chemistry Reviews* **2013,** *257*, 2468-2483.
26. Haberlen, O. D.; Rosch, N., Effect of Phosphine Substituents in Gold(I) Complexes - a Theoretical-Study of Meaupr3, R = H, Me, Ph. *J Phys Chem-Us* **1993,** *97* (19), 4970-4973.

27. Ivanov, S. A.; Arachchige, I.; Aikens, C. M., Density Functional Analysis of Geometries and Electronic Structures of Gold-Phosphine Clusters. The Case of Au-4(PR3)(4)(2+) and Au-4(mu(2)-I)(2)(PR3)(4). *J Phys Chem A* **2011,** *115* (27), 8017-8031.
28. Golightly, J. S.; Gao, L.; Castleman, A. W.; Bergeron, D. E.; Hudgens, J. W.; Magyar, R. J.; Gonzalez, C. A., Impact of swapping ethyl for phenyl groups on diphosphine-protected undecagold. *J Phys Chem C* **2007,** *111* (40), 14625-14627.
29. Hudgens, J. W.; Pettibone, J. M.; Senftle, T. P.; Bratton, R. N., Reaction Mechanism Governing Formation of 1,3-Bis(diphenylphosphino)propane-Protected Gold Nanoclusters. *Inorganic Chemistry* **2011,** *50* (20), 10178-10189.
30. Pettibone, J. M.; Hudgens, J. W., Synthetic Approach for Tunable, Size-Selective Formation of Monodisperse, Diphosphine-Protected Gold Nanoclusters. *J Phys Chem Lett* **2010,** *1* (17), 2536-2540.
31. Ligare, M. R.; Johnson, G. E.; Laskin, J., Observing the real time formation of phosphine-ligated gold clusters by electrospray ionization mass spectrometry. . *Phys. Chem. Chem. Phys.* **2017,** *19* (26), 17187-17198.
32. Johnson, G. E.; Priest, T.; Laskin, J., Synthesis and Characterization of Gold Clusters Ligated with 1,3-Bis(dicyclohexylphosphino)propane. *Chempluschem* **2013,** *78* (9), 1033-1039.
33. Jin, R. C., Quantum sized, thiolate-protected gold nanoclusters. *Nanoscale* **2010,** *2* (3), 343-362.
34. Negishi, Y.; Sakamoto, C.; Ohyama, T.; Tsukuda, T., Synthesis and the Origin of the Stability of Thiolate-Protected Au-130 and Au(187)Clusters. *J Phys Chem Lett* **2012,** *3* (12), 1624-1628.
35. Mingos, D. M. P., STRUCTURE AND BONDING IN CLUSTER COMPOUNDS OF GOLD. *Polyhedron* **1984,** *3* (12), 1289-1297.
36. Weare, W. W.; Reed, S. M.; Warner, M. G.; Hutchison, J. E., Improved synthesis of small (d(CORE) approximate to 1.5 nm) phosphine-stabilized gold nanoparticles. *J Am Chem Soc* **2000,** *122* (51), 12890-12891.
37. Johnson, G. E.; Priest, T.; Laskin, J., Size-dependent stability toward dissociation and ligand binding energies of phosphine ligated gold cluster ions. *Chem Sci* **2014,** *5* (8), 3275-3286.
38. Johnson, G. E.; Laskin, J., Understanding ligand effects in gold clusters using mass spectrometry. *Analyst* **2016,** *141* (12), 3573-3589.
39. Shafai, G.; Hong, S. Y.; Bertino, M.; Rahman, T. S., Effect of Ligands on the Geometric and Electronic Structure of Au-13 Clusters. *J Phys Chem C* **2009,** *113* (28), 12072-12078.
40. Hong, S.; Shafai, G.; Bertino, M.; Rahman, T. S., Toward an Understanding of Ligand Selectivity in Nanocluster Synthesis. *J Phys Chem C* **2011,** *115* (30), 14478-14487.
41. Mollenhauer, D.; Gaston, N., A Balanced Procedure for the Treatment of Cluster-Ligand Interactions on Gold Phosphine Systems in Catalysis. *J. Comput. Chem.* **2014,** *35* (13), 986-997.
42. Johnson, G. E.; Olivares, A.; Hill, D.; Laskin, J., Cationic gold clusters ligated with differently substituted phosphines: effect of substitution on ligand reactivity and binding. *Phys. Chem. Chem. Phys.* **2015,** *17* (22), 14636-14646.
43. Pettibone, J. M.; Hudgens, J. W., Gold Cluster Formation with Phosphine Ligands: Etching as a Size-Selective Synthetic Pathway for Small Clusters? *Acs Nano* **2011,** *5* (4), 2989-3002.
44. Bergeron, D. E.; Coskuner, O.; Hudgens, J. W.; Gonzalez, C. A., Ligand exchange reactions in the formation of diphosphine-protected gold clusters. *J Phys Chem C* **2008,** *112* (33), 12808-12814.
45. Armentrout, P. B., Gas-phase perspective on the thermodynamics and kinetics of heterogeneous catalysis. *Catal Sci Technol* **2014,** *4* (9), 2741-2755.
46. Walter, M.; Akola, J.; Lopez-Acevedo, O.; Jadzinsky, P. D.; Calero, G.; Ackerson, C. J.; Whetten, R. L.; Gronbeck, H.; Hakkinen, H., A unified view of ligand-protected gold clusters as superatom complexes. *Proc. Natl. Acad. Sci. U. S. A.* **2008,** *105* (27), 9157-9162.
47. Bellon, P. L.; Cariati, F.; Manasser.M; Naldini, L.; Sansoni, M., Novel Gold Clusters - Preparation, Properties, and X-Ray Structure Determination of Salts of Octakis(Triarylphosphine)Enneagold, [Au9l8]X3. *J Chem Soc Chem Comm* **1971,** (22), 1423-&.
48. Bellon, P.; Manasser.M; Sansoni, M., Octahedral Gold Cluster - Crystal and Molecular-Structure of Hexakis-[Tris-(P-Tolyl)Phosphine)-Octahedro-Hexagold Bis(Tetraphenylborate). *J Chem Soc Dalton* **1973,** (22), 2423-2427.
49. Mingos, M., *Gold Clusters, Colloids and Nanoparticles I*. Springer: Switzerland, 2014; Vol. 161.
50. Vollenbroek, F. A.; Bosman, W. P.; Bour, J. J.; Noordik, J. H.; Beurskens, P. T., REACTIONS OF GOLD-PHOSPHINE CLUSTER COMPOUNDS - PREPARATION AND X-RAY STRUCTURE DETERMINATION OF OCTAKIS(TRIPHENYLPHOSPHINE)-OCTA-GOLD BIS-(HEXAFLUOROPHOSPHATE). *J. Chem. Soc.-Chem. Commun.* **1979,** (9), 387-388.
51. Briant, C. E.; Theobald, B. R. C.; White, J. W.; Bell, L. K.; Mingos, D. M. P.; Welch, A. J., Synthesis and X-Ray Structural Characterization of the Centered Icosahedral Gold Cluster Compound [Au13(Pme2ph)10cl2](Pf6)3 - the Realization of a Theoretical Prediction. *J. Chem. Soc.-Chem. Commun.* **1981,** (5), 201-202.
52. Briant, C. E.; Hall, K. P.; Wheeler, A. C.; Mingos, D. M. P., Structural Characterization of [Au10cl3(Pcy2ph)6](No3) (Cy = Cyclohexyl) and the Development of a Structural Principle for High Nuclearity Gold Clusters. *J. Chem. Soc.-Chem. Commun.* **1984,** (4), 248-250.
53. Vandervelden, J. W. A.; Vollenbroek, F. A.; Bour, J. J.; Beurskens, P. T.; Smits, J. M. M.; Bosman, W. P., Gold Clusters Containing Bidentate Phosphine-Ligands - Preparation and X-Ray Structure Investigation of [Au5(Dppmh)3(Dppm)](No3)2 and [Au13(Dppmh)6](No3)N. *Recl Trav Chim Pay B* **1981,** *100* (4), 148-152.

54. Fey, N.; Tsipis, A. C.; Harris, S. E.; Harvey, J. N.; Orpen, A. G.; Mansson, R. A., Development of a ligand knowledge base, Part 1: Computational descriptors for phosphorus donor ligands. *Chem-Eur J* **2006,** *12* (1), 291-302.
55. Suresh, C. H., Molecular electrostatic potential approach to determining the steric effect of phosphine ligands in organometallic chemistry. *Inorganic Chemistry* **2006,** *45* (13), 4982-4986.
56. Hamouda, R.; Bertorelle, F.; Rayane, D.; Antoine, R.; Broyer, M.; Dugourd, P., Glutathione capped gold Au-N(SG)(M) clusters studied by isotope-resolved mass spectrometry. *Int J Mass Spectrom* **2013,** *335*, 1-6.
57. Niihori, Y.; Kurashige, W.; Matsuzaki, M.; Negishi, Y., Remarkable enhancement in ligand-exchange reactivity of thiolate-protected Au-25 nanoclusters by single Pd atom doping. *Nanoscale* **2013,** *5* (2), 508-512.
58. Fields-Zinna, C. A.; Sampson, J. S.; Crowe, M. C.; Tracy, J. B.; Parker, J. F.; deNey, A. M.; Muddiman, D. C.; Murray, R. W., Tandem Mass Spectrometry of Thiolate-Protected Au Nanoparticles NaxAu25(SC2H4Ph)(18-y)(S(C2H4O)(5)CH3)(y). *J Am Chem Soc* **2009,** *131* (38), 13844-13851.
59. Zavras, A.; Khairallah, G. N.; O'Hair, R. A. J., Bis(diphenylphosphino)methane ligated gold cluster cations: Synthesis and gas-phase unimolecular reactivity. *Int J Mass Spectrom* **2013,** *354*, 242-248.
60. Olivares, A.; Laskin, J.; Johnson, G. E., Investigating the Synthesis of Ligated Metal Clusters in Solution Using a Flow Reactor and Electrospray Ionization Mass Spectrometry. *J Phys Chem A* **2014,** *118* (37), 8464-8470.
61. Pettibone, J. M.; Hudgens, J. W., Predictive Gold Nanocluster Formation Controlled by Metal-Ligand Complexes. *Small* **2012,** *8* (5), 715-725.
62. Robinson, P. S. D.; Nguyen, T. L.; Lioe, H.; O'Hair, R. A. J.; Khairallah, G. N., Synthesis and gas-phase uni- and bi-molecular reactivity of bisphosphine ligated gold clusters, AuxLy (n+). *Int J Mass Spectrom* **2012,** *330*, 109-117.
63. Niihori, Y.; Kikuchi, Y.; Kato, A.; Matsuzaki, M.; Negishi, Y., Understanding Ligand-Exchange Reactions on Thiolate-Protected Gold Clusters by Probing Isomer Distributions Using Reversed-Phase High-Performance Liquid Chromatography. *Acs Nano* **2015,** *9* (9), 9347-9356.
64. Pan, S.; Saha, R.; Mandal, S.; Chattaraj, P. K., σ-Aromatic cyclic M_3^+ (M = Cu, Ag, Au) clusters and their complexation with dimethyl imidazol-2-ylidene, pyridine, isoxazole, furan, noble gases and carbon monoxide. *Phys. Chem. Chem. Phys.* **2016,** *18*, 11661-11676.
65. Robinson, P. S. D.; Khairallah, G. N.; da Silva, G.; Lioe, H.; O'Hair, R. A. J., Gold-Mediated C-I Bond Activation of Iodobenzene. *Angewandte Chemie International Edition* **2012,** *51*, 3812-3817.
66. Mollenhauer, D., Nitrogen- and phosphine-binding ligands in interaction with gold atoms, clusters, nanoparticles and surfaces. *Chemical Modelling* **2016,** *12*, 293-350.
67. Robilotto, T. J.; Bacsa, J.; Gray, T. G.; Sadighi, J. P., Synthesis of a Trigold Monocation: An Isolobal Analogue of $[H_3]^+$. *Angew. Chem. Int. Ed.* **2012,** *51*, 12077-12080.
68. Bertino, M. F.; Sun, Z.-M.; Zhang, R.; Wang, L.-S., Facile Syntheses of Monodisperse Ultrasmall Au Clusters. *J Phys Chem B* **2006,** *110*, 21416-21418.
69. Frisch, M. J. T., G. W.; Schlegel, H. B.; Scuseria, G. E.; Robb, M. A.; Cheeseman, J. R.; Scalmani, G.; Barone, V.; Mennucci, B.; Petersson, G. A.; Nakatsuji, H.; Caricato, M.; Li, X.; Hratchian, H. P.; Izmaylov, A. F.; Bloino, J.; Zheng, G.; Sonnenberg, J. L.; Hada, M.; Ehara, M.; Toyota, K.; Fukuda, R.; Hasegawa, J.; Ishida, M.; Nakajima, T.; Honda, Y.; Kitao, O.; Nakai, H.; Vreven, T.; Montgomery, J. A., Jr.; Peralta, J. E.; Ogliaro, F.; Bearpark, M.; Heyd, J. J.; Brothers, E.; Kudin, K. N.; Staroverov, V. N.; Kobayashi, R.; Normand, J.; Raghavachari, K.; Rendell, A.; Burant, J. C.; Iyengar, S. S.; Tomasi, J.; Cossi, M.; Rega, N.; Millam, J. M.; Klene, M.; Knox, J. E.; Cross, J. B.; Bakken, V.; Adamo, C.; Jaramillo, J.; Gomperts, R.; Stratmann, R. E.; Yazyev, O.; Austin, A. J.; Cammi, R.; Pomelli, C.; Ochterski, J. W.; Martin, R. L.; Morokuma, K.; Zakrzewski, V. G.; Voth, G. A.; Salvador, P.; Dannenberg, J. J.; Dapprich, S.; Daniels, A. D.; Farkas, Ö.; Foresman, J. B.; Ortiz, J. V.; Cioslowski, J.; Fox, D. J. Gaussian, Inc., Wallingford CT, 2013, Gaussian 09, Revision E.01. 2013, Gaussian 09, Revision E.01. **2013**.
70. Becke, A. D., Density-Functional Thermochemistry .3. The Role of Exact Exchange. *J Chem Phys* **1993,** *98* (7), 5648-5652.
71. Lee, C. T.; Yang, W. T.; Parr, R. G., Development of the Colle-Salvetti Correlation-Energy Formula into a Functional of the Electron-Density. *Phys Rev B* **1988,** *37* (2), 785-789.
72. Stephens, P. J.; Devlin, F. J.; Chabalowski, C. F.; Frisch, M. J., Ab-Initio Calculation of Vibrational Absorption and Circular-Dichroism Spectra Using Density-Functional Force-Fields. *J Phys Chem-Us* **1994,** *98* (45), 11623-11627.
73. Dunning Jr., T. H. H., P.J., Modern Theoretical Chemistry, Ed. H.F. Schaefer III, Vol. 3. *Plenum, New York* **1977**, 1-28.
74. Glendening, E. D. B., J.K.; Reed,A.E.; Carpenter, J.E.; Bohmann, J.A.; Morales, C.M.; Landis, C.M.; Weinhold,F., http://nbo6.chem.wisc.edu. *Theoretical Chemistry Institute, University of Wisconsin, Madison, WI* **2013**.